NOISE CONTROL IN DUCTS USING PERIODIC HELMHOLTZ RESONATORS

Conference Paper · January 2017

DOI: 10.20906/CPS/CILAMCE2017-0425

3 authors, including:

J. M. C. Dos Santos
University of Campinas
80 PUBLICATIONS **117** CITATIONS

SEE PROFILE

NOISE CONTROL IN DUCTS USING PERIODIC HELMHOLTZ RESONATORS

Brenno V. L. Campos
Audrey Babinet
José Maria C. Dos Santos
brennovictor.lc@outlook.com
Audrey.Babinet.Etu@univ-lemans.fr
zema@fem.unicamp.br
University of Campinas, UNICAMP-FEM-DMC, Mendeleiev street, 200, Cidade Universitária "Zeferino Vaz", Barão Geraldo, Postal Code 13083-860, Campinas (SP), Brazil

Abstract. *Helmholtz resonators have been used extensively in acoustic engineering as passive devices to reduce noise in narrow frequency bands. In the last decades, some approaches have been proposed to improve the performance of Helmholtz resonator. Many of them concentrate on tuning the resonance frequency to enlarge the resonance bandwidth and improve the transmission loss. To broaden the frequency bandwidth, configurations of Helmhlotz resonator in array are proposed. An interesting and promising approach to obtain a broader attenuation range in a duct consists in to distribute local resonators branch-side type with Helmholtz resonators periodically along the duct. This generates some frequency bands, known as "stop bands" or "band gaps", were harmonic waves do not propagate. Bandgaps commonly studied in the area of phononic crystals and metamaterials are generated based on the spatial frequency of mismatched impedance areas which produce Bragg scattering effect and local resonance effect from the Helmholtz resonators. This work investigates the band gaps created in duct-resonator system using acoustic transfer matrix method (TMM) and wave finite element (WFE) models. Periodic geometry variations are investigated. The Floquet-Bloch theorem is used on a transfer matrix of the periodic cell rearranged from an acoustic dynamic stiffness matrix to obtain the dispersion diagrams that reveal the band gaps caused by Bragg scattering and local resonance numerical predictions of the dispersion ratio of a duct-resonator system are compared with a TMM and WFE model.*

Keywords: *Bandgaps, helmholtz resonator, duct, noise control, TMM. WFE.*

Proceedings of the XXXVIII Iberian Latin-American Congress on Computational Methods in Engineering P.O. Faria, R.H. Lopez, L.F.F. Miguel, W.J.S. Gomes, M. Noronha (Editores), ABMEC, Florianópolis, SC, Brazil, November 5-8, 2017.

1 INTRODUCTION

The use of acoustical silencers is widely applied for noise control in combustion engines and ventilation systems. Helmholtz resonators (HR) have been used extensively in acoustic engineering as passive devices to reduce noise in narrow frequency bands. In the last decades, some approaches have been proposed to improve the performance of Helmholtz resonator. They are concentrated on tuning the resonance frequency to enlarge the resonance bandwidth and improve the transmission loss. Configurations of HR in array have been proposed to enlarge the frequency bandwidth,. An approach to broader attenuation range in a duct consists in to distribute HR's periodically along the duct. This generates some frequency bands, known as prohibited bands or bandgaps, were harmonic waves do not propagate. Commonly studied in the area of phononic crystals and metamaterials, bandgaps are generated based on the spatial frequency of mismatched impedance areas which produce Bragg scattering effect and/or local resonance effect from the HR's.

This paper investigates the bandgaps created in duct-HR periodic system using acoustic transfer matrix method (TMM) and wave finite element (WFE) method. Periodic geometry variations are investigated. The TMM is based on the plane wave acoustic formulation for a duct-HR unit-cell to obtain a transfer matrix (Munjal, 1987). In the following, Floquet-Bloch theorem is applied on the transfer matrix to obtain an eigenvalue problem, whose solutions are the wavenumbers (dispersion diagrams) and the corresponding wave modes (wave amplitudes) caused by Bragg scattering and local resonance.

Recently developed to evaluate the behavior of periodic structures from a unit cell modeled by finite element (FE) method, the WFE (Ichchou and Mencik , 2005) is applied here to calculate bandgaps in a duct-HR acoustic system. In this method the dynamic stiffness matrix of a unit-cell of the duct-HR acoustic system is modeled by FE and transformed in the transfer matrix form. Using Floquet-Bloch's theorem results in an eigenvalue/vector problem, whose solution gives the wavenumbers and the corresponding wave modes. WFE has been used for free and forced wave propagation in vibration analysis (Duhamel, 2006) with applications to one and two-dimensional structural models (Mace and Maconi, 2008). Here, WFEM will be applied to model acoustic metamaterial waveguide with Helmholtz local resonators.

Numerical predictions of the dispersion diagrams of a periodic duct-HR system calculated by TMM model and WFE with 2D, 3D and 3D-fractioned models are compared. An important result of this paper is to demonstrate the accuracy, flexibility and efficiency of WFE for modeling acoustic metamaterial system.

2 ACOUSTIC METAMATERIAL MODELLING

Let's consider the metamaterial acoustic duct with spatial periodic distribution and periodically attached acoustic Helmholtz local resonators, as sketched in Figure 1. The length of each unit-cell is L. For the spatial periodic distribution the band gaps are generated by Bragg scattering, which appears around frequencies governed by $L = n(\lambda/2)$ (n = 1,2,...). The local resonators are represented by a series of Helmholtz resonators, HR_n with n = 1, 2, ..., N

where N is the number of HR. The local resonator bandgap appear around the natural frequency of HR given by.

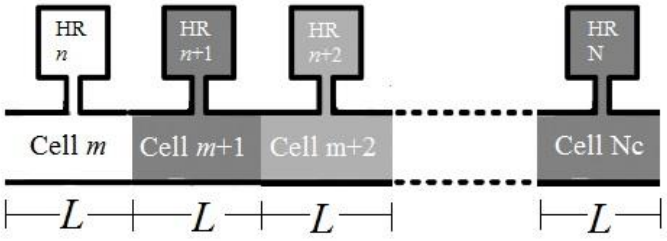

Figure 1. Periodic acoustic duct with local Helmholtz resonators.

Considering that the acoustic metamaterial unit-cell consists of an acoustic duct connected with a local Helmholtz resonator, by using Floquet-Bloch theorem it can be modeled for only one unit-cell to obtain the wave numbers (dispersion diagram) and the corresponding wave modes (wave amplitudes).

2.1 Transfer Matrix Model

The TMM has been widely used as a tool for calculate complex systems due to its computational efficiency and flexibility. Some researchers (Munjal 1987, Singh *et al.*, 2008) have used the TMM for analyzing acoustic duct systems. Although many research papers and acoustic text books (Beranek and Ver 1992, Kinsler et al. 1992), provide a brief outline of the TMM, they do not include some important details of a particular system.

In order to model the unit-cell of the acoustic duct attached to a HR using TMM, it is applied a similar modeling as presented by Singh *et al.* (2008). It consists in divide the duct-HR systems in three elements: Element D1 - part of the duct before the HR; Element D2 - part of the duct after the HR, and Element HR - the Helmholtz resonator. Figure 2 shows a sketch of the unit-cell duct-HR of length L with the HR at the location x. The figure also indicates the three Elements D1, D2 and HR, along with the neck-cavity and neck-duct interfaces.

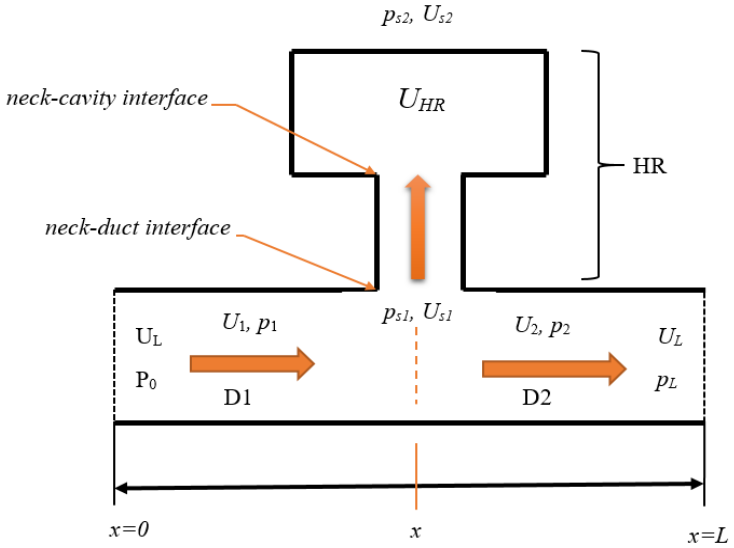

Figure 2. Sketch of the unit-cell duct-HR system.

The transfer matrix of a duct can be obtained from a 1D acoustic model. The non-dissipative wave equation can written as (Kinsley, 1982):

$$\frac{\partial^2 p}{\partial x^2} = \frac{1}{c^2}\frac{\partial^2 p}{\partial t^2} \tag{1}$$

where p is the acoustic pressure, c is the sound velocity, x is the space and t is the time. The solution of Eq. (1) can be written as,

$$p(x) = Ae^{-jkx} + Be^{jkx} \tag{2}$$

where, A and B are complex coefficients to be determined by boundary conditions, j is the imaginary unit, $k = \omega/c$ is the wave number, ω is the circular frequency.

By substituting Eq.(2) in the Euler equation, $u(x) = -\frac{1}{\rho}\int \frac{\partial p}{\partial x}$, particle velocity can be obtained as:

$$u(x) = \frac{1}{\rho c}\left(Ae^{-jkx} - Be^{jkx}\right) \tag{3}$$

where ρ is the air density. Rewriting particle velocity as volume velocity it has:

$$U(x) = \frac{S_d}{\rho c}\left(Ae^{-jkx} - Be^{jkx}\right) \tag{4}$$

where S_d is the duct cross section. From Eqs. (2) and (4) the transfer matrix of a circular duct of uniform cross section area S_d and length, l, can be written as (Munjal, 1987):

$$\begin{Bmatrix} U_n \\ p_n \end{Bmatrix} = \begin{bmatrix} cos(\hat{k}l) & j\frac{S_d}{\rho c}sin(\hat{k}l) \\ j\frac{\rho c}{S_d}sin(\hat{k}l) & cos(\hat{k}l) \end{bmatrix} \begin{Bmatrix} U_{n-1} \\ p_{n-1} \end{Bmatrix} \tag{5}$$

where $\hat{k} = k(1 + j\eta)$ is a complex wave number that was formulated to include damping in the system and η is the loss factor. The subscripts, n and n–1, represent the extreme ends of the duct, input and output sides, respectively. Let's consider a duct with the input end (source) at $x = 0$, output end (open) at $x = L$, and the effective length of the duct l_e, then Eq. (5) becomes:

$$\begin{Bmatrix} U_0 \\ p_0 \end{Bmatrix} = \begin{bmatrix} cos(\hat{k}l_e) & j\frac{S_d}{\rho c}sin(\hat{k}l_e) \\ j\frac{\rho c}{S_d}sin(\hat{k}l_e) & cos(\hat{k}l_e) \end{bmatrix} \begin{Bmatrix} U_L \\ p_L \end{Bmatrix} \tag{6}$$

The effective length is $l_e = L + 0.6a$, which corresponds to the sum of physical duct length, L, and the end-correction factor, $0.6a$. This end-correction factor is for a duct with an unflanged open end, where a is the duct's radius (Kinsler *et al.*, 1994). Equation (6) can be written in a compact form as:

$$\mathbf{q}_0 = \mathbf{T}_d \mathbf{q}_L \tag{7}$$

where $\mathbf{T}_d$ is the *duct transfer matrix* and $\mathbf{q}_0$ and $\mathbf{q}_L$ are the state vector at position $x = 0$ and L, respectively.

By applying continuity and compatibility conditions for the volume velocity and acoustic pressure in the duct-HR model (Figure 2), it is obtained:

$$U_1(x) = U_{HR}(x) + U_2(x) \tag{8}$$
$$p_1(x) = p_{HR}(x) = p_2(x) \tag{9}$$

Rewriting Eq. (8) and (9) in matrix form it has:

$$\begin{Bmatrix} U_1 \\ p_1 \end{Bmatrix} = \begin{bmatrix} U_{HR} + U_L \\ p_L \end{bmatrix} \tag{10}$$

$$\begin{Bmatrix} U_1 \\ p_1 \end{Bmatrix} = \begin{bmatrix} 1 & U_{HR}/p_L \\ 0 & 1 \end{bmatrix} \begin{Bmatrix} U_L \\ p_L \end{Bmatrix} \tag{11}$$

From Eq. (9), $p_L(x) = p_{HR}(x)$, so we have, $\frac{p_{HR}}{U_{HR}} = Z_{HR}$, which is the HR acoustic impedance just outside the opening of the resonator. Then, also from Eq. (9), the Eq. (11) can be rewritten as:

$$\begin{Bmatrix} u_0 \\ p_0 \end{Bmatrix} = \begin{bmatrix} 1 & \frac{1}{Z_{HR}} \\ 0 & 1 \end{bmatrix} \begin{Bmatrix} u_L \\ p_L \end{Bmatrix} \tag{12}$$

Equation (12) can also be written in a compact form as:

$$\mathbf{q}_0 = \mathbf{T}_{HR} \mathbf{q}_L \tag{13}$$

where $\mathbf{T}_{HR}$ is the *Helmholtz resonator transfer matrix* and $\mathbf{q}_0$ and $\mathbf{q}_L$ are the state vector at position $x = 0$ and l, respectively.

Now the three Elements D1, D2 and HR can be assembling together to obtain the transfer matrix of the unit-cell duct-HR. The transfer matrix resulting is the product of the transfer matrix of each element. Then, form Eq. (7) applied to the elements D1 and D2 and Eq. (11) applied to the HR element, it is obtained as:

$$\mathbf{q}_0 = \mathbf{T}_{d1} \mathbf{T}_{HR} \mathbf{T}_{d2} \mathbf{q}_L \quad \text{or} \quad \mathbf{q}_0 = \mathbf{T}_{dHR} \mathbf{q}_L \tag{14}$$

where $\mathbf{T}_{dHR}$ is the *unit-cell duct-HR transfer matrix*. Before apply periodicity condition Eq. (14) can be rewritten in a more convenient form as:

Proceedings of the XXXVIII Iberian Latin-American Congress on Computational Methods in Engineering P.O. Faria, R.H. Lopez, L.F.F. Miguel, W.J.S. Gomes, M. Noronha (Editores), ABMEC, Florianópolis, SC, Brazil, November 5-8, 2017.

$$\mathbf{q}_r = \mathbf{T}_{dHR}\mathbf{q}_L \tag{15}$$

where $\mathbf{q}_r$ and $\mathbf{q}_l$ now are the state vector at the right and left position of the unit-cell, respectively. Let's consider now consecutive unit-cells, *m* and *m*+1, in the structure shown in Fig. 1. The volume velocity and acoustic pressure compatibility and continuity condition produces $\mathbf{q}_r^{(m)} = \mathbf{q}_L^{(m+1)}$. By substituting in Eq. (15), produces:

$$\mathbf{q}_L^{(m+1)} = \mathbf{T}_{dHR}\mathbf{q}_L^{(m)} \tag{16}$$

The Floquet-Bloch theorem for wave propagation in an infinite periodic system applied to consecutive unit-cells, generates:

$$\mathbf{q}_L^{(m+1)} = \mathrm{e}^{\mu}\mathbf{q}_L^{(m)} \tag{17}$$

where $\mu = -jkL$ is the attenuation constant. Substituting Eq. (17) in Eq. (16) and rearranging, it has:

$$\mathbf{T}_{dHR}\mathbf{q}_L^{(m)} = \mathrm{e}^{\mu}\mathbf{q}_L^{(m)} \quad \text{or} \quad \mathbf{T}_{dHR}\mathbf{q}_L = \mathrm{e}^{\mu}\mathbf{q}_L \tag{18}$$

which is the Bloch wave eigenvalue/vector problem, where e^{μ} is the Bloch wave number and $\mathbf{q}_L$ are the corresponding wave vectors.

3 Wave Finite Element Model

Equation (1) can be written in a more complete form as:

$$\nabla^2\mathbf{p} = \frac{1}{c^2}\frac{\partial^2\mathbf{p}}{\partial t^2} \tag{19}$$

where ∇ is the differential operator and $\mathbf{p}$ is a vector in the space R^3.

The acoustic pressure field in a duct-HR system excited by plane waves can be modeled as 2D and 3D problem. To solve Eq. (19) in a specified volume, boundary conditions must be applied at its surface boundaries. For a solid surface, the boundary condition is given by,

$$\frac{\partial\mathbf{p}}{\partial\mathbf{n}} = \rho\ddot{\mathbf{u}}_\mathbf{n} \tag{20}$$

where $\mathbf{n}$ is the outward unit surface normal and $\ddot{\mathbf{u}}_\mathbf{n}$ is the boundary acceleration in the direction $\mathbf{n}$.

This boundary value problem is usually solved by finite element analysis, using Galerkin's Method to obtain an approximated solution (Cook *et al.*, 2002). After discretization, the system of equations to be solved is

$$\mathbf{M}_a\ddot{\mathbf{p}} - \mathbf{K}_a\mathbf{p} = \mathbf{f} \tag{21}$$

where $\mathbf{M}_a$ is the acoustic mass matrix, $\mathbf{K}_a$ is the acoustic stiffness matrix, $\mathbf{f}$ is the acoustic excitation vector and $\mathbf{p}$ is the acoustic pressure nodal vector. The mass and stiffness matrices are obtained from the commercial software ANSYS® using acoustic models 2D, 3D and fractional 3D.

The acoustic dynamic stiffness matrix can be written as:

$$\mathbf{D} = \mathbf{K}_a - \omega^2 \mathbf{M}_a \tag{22}$$

which can be partitioned in terms of internal, left-side and right-side degrees of freedom by

$$\begin{bmatrix} \mathbf{D_{ii}} & \mathbf{D_{il}} & \mathbf{D_{ir}} \\ \mathbf{D_{li}} & \mathbf{D_{ll}} & \mathbf{D_{lr}} \\ \mathbf{D_{ri}} & \mathbf{D_{rl}} & \mathbf{D_{rr}} \end{bmatrix} \begin{Bmatrix} \mathbf{p_i} \\ \mathbf{p_l} \\ \mathbf{p_r} \end{Bmatrix} = \begin{Bmatrix} \mathbf{0_i} \\ \mathbf{f_l} \\ \mathbf{f_r} \end{Bmatrix} \tag{23}$$

From Eq. (23) the internal pressures can be written as:

$$\mathbf{p_i} = \mathbf{D_{ii}^{-1}}(\mathbf{D_{il}}\mathbf{p_l} + \mathbf{D_{ir}}\mathbf{p_r}) \tag{24}$$

Substituting Eq. (24) into Eq. (23) the condensed acoustic dynamic stiffness matrix is obtained as:

$$\begin{bmatrix} \mathbf{D_{ll}} & \mathbf{D_{lr}} \\ \mathbf{D_{rl}} & \mathbf{D_{rr}} \end{bmatrix} \begin{Bmatrix} \mathbf{p_l} \\ \mathbf{p_r} \end{Bmatrix} = \begin{Bmatrix} \mathbf{f_l} \\ \mathbf{f_r} \end{Bmatrix} \tag{25}$$

where, $\mathbf{D_{ll}} = \mathbf{D_{ll}} - \mathbf{D_{li}^{-1}}\mathbf{D_{il}}$, $\mathbf{D_{rl}} = \mathbf{D_{rl}} - \mathbf{D_{ri}}\mathbf{D_{ii}^{-1}}\mathbf{D_{il}}$, $\mathbf{D_{rl}} = \mathbf{D_{lr}} - \mathbf{D_{li}}\mathbf{D_{ii}}$ and $\mathbf{D_{rr}} = \mathbf{D_{rr}} - \mathbf{D_{ri}}\mathbf{D_{ii}^{-1}}\mathbf{D_{ir}}$.

In this method the dynamic stiffness matrix of a unit-cell of the whole structure, modeled by FE is used to apply the periodicity condition in a harmonic disturbance propagating through the duct-HR system. Rearranging the Eq.(25) as the transfer matrix formulation one produces:

$$\begin{Bmatrix} \mathbf{p_r} \\ -\mathbf{f_r} \end{Bmatrix} = \begin{bmatrix} -\mathbf{D_{lr}^{-1}}\mathbf{D_{ii}} & -\mathbf{D_{lr}} \\ \mathbf{D_{rl}} - \mathbf{D_{rr}}\mathbf{D_{rl}^{-1}}\mathbf{D_{ll}} & -\mathbf{D_{rr}^{-1}}\mathbf{D_{lr}} \end{bmatrix} \begin{Bmatrix} \mathbf{p_l} \\ \mathbf{f_l} \end{Bmatrix} \quad \text{or} \quad \mathbf{q}_r = \mathbf{T}_{WFE}\mathbf{q}_l \tag{26}$$

where $\mathbf{T}_{WFE}$ is the *unit-cell duct-HR transfer matrix* obtained by WFE.

Considering that Eqs. (26) and (15) are similar the same procedure to apply Foquet-Bloch theorem in the Eq.(15) can be used for the Eq. (26) to obtain a similar eigenproblem. given now by

$$\mathbf{T}_{WFE}\mathbf{q}_L = e^{\mu}\mathbf{q}_L \tag{27}$$

4 SIMULATED RESULTS

In this section some simulated example are evaluated in order to compare the TMM and WFE methods. A first FE model of the unit-cell of the acoustic duct-HR, called Model 1, was designed in ANSYS software with the three geometries: 2D, 3D, and fractioned 3D from now on called F3D. Figure 3 shows the aspect of these geometries. The values of geometric parameters and material properties presented in Table 1 are the same for all models of unit-cell duct-HR. Only the parameter cavity length will vary for different models. For the Model 1 it is lc = 0.2 m. All models are discretized with element type FLUID29 (triangular) for 2D geometry, and element type FLUID30 (tetrahedral) for 3D geometry. Mesh free generation is applied for all models.

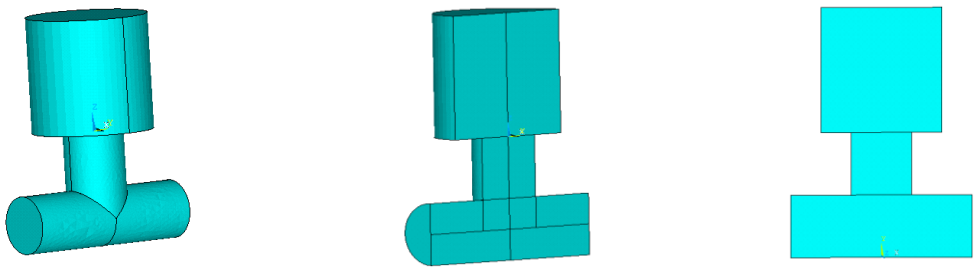

(a) (b) (c)

Figure 3. Model 1 designed in ANSYS for the unit-cell model with geometry: (a) 3D; (b) F3D; and (c) 2D.

Table 1. Geometric parameters and air properties for all unit-cell models.

Geometry/Property	Value
Unit-cell length (L)	0.3 m
Neck length (ln)	0.1 m
Duct diameter (D)	0.1 m
Neck diameter (dn)	0.1 m
Cavity diameter (dc)	0.2 m
Sound velocity (c)	343.24 m/s
Air density (ρ)	1.2041 kg/m^3

Figure 4 shows the mesh free generated by ANSYS software for the Model 1, with the restriction of 15 elements/wavelength for the geometry: 3D, F3D and 2D. Table 2 shows the number of nodes and elements generated in the models.

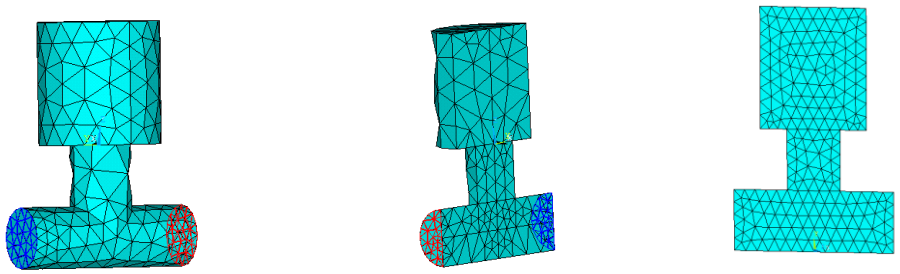

(a) (b) (c)

Figure 4. Model 1 mesh generated by ANSYS with geometry: (a) 3D; (b) F3D; (c) 2D.

Table 2. Number of nodes and elements in Model 1.

Geometry	Elements	Nodes
3D	1530	438
F3D	819	305
2D	405	242

Figure 5 shows the dispersion diagram for the Model 1, which presents together the real part (propagative waves) and the negative of imaginary part (non-propagative or evanescent waves) of *kL* versus frequency.

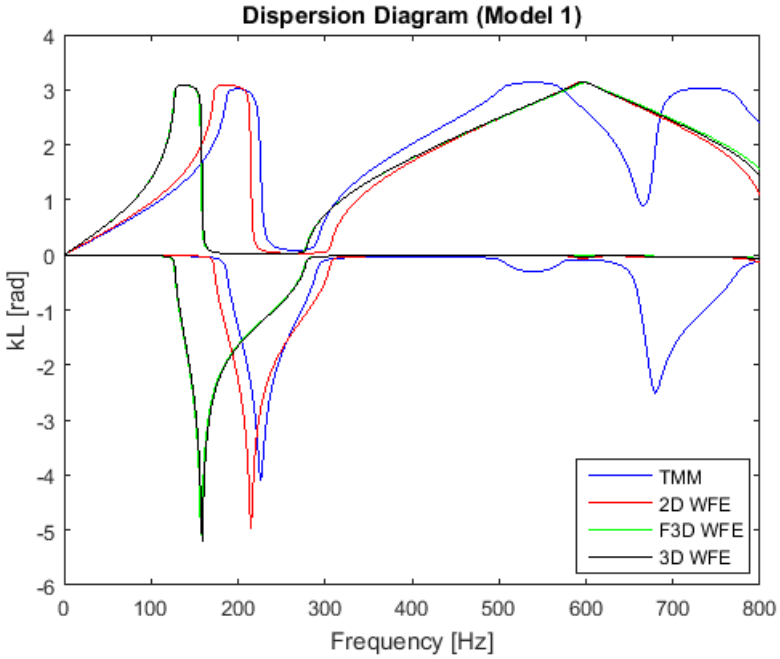

Figure 5. Dispersion diagram for Model 1 calculated by TMM and WFE with geometry: 2D, F3D and 3D.

At low frequency band both methods (TMM and WFE) agrees, however as the frequency band increase TMM and WFE with all geometries (2D, 3D and F3D) diverges. As expected WFE-3D and WFE-F3D presents a good agreement for all frequency band, and WFE-2D becomes close to the formers as the frequency increases. Since the bandgaps represents the non-propagative waves they will be located in the negative imaginary part of *kL* in the graphic. It can be seen two band gaps, the first one can be identified as a locally resonant bandgap which occur around the natural frequency of the HR (f_{HR} = 193.14 Hz). The second one is a bandgap from the periodicity, which is located around the Bragg limit of f_{BL} = 572.1 Hz. It can be seen that both methods can identify the bandgap but presents a difference in the bandgap position and width obtained with TMM & WFE-2D as compared to the WFE-3D & F3D, which are coincident. Also the TMM identifies a third bandgap around the frequency of 700 Hz, which is not correct and seems to be the TMM limit, considering the plane wave hypothesis was assumed in the formulations.

4.1 HR Cavity Geometry Variation

Another way to explore the bandgap behavior is to vary the cavity volume of HR. It was performed by varying the cavity length (*lc*) in order to evaluate this parameter sensitivity related to bandgap width and position. For this purpose the Model 1 had his cavity length reduced to the half, i.e. *lc* = 0.1 m, and becomes Model 2. Figure 5 shows the Model 2 mesh generated by ANSYS with geometry: 3D, F3D and 2D. Table 3 shows the number of nodes and elements used for each geometry (3D, F3D and 2D) of Model 2. describes the dimensions for 3D, fractional 3D and 2D models to compare the results obtained by dispersion relation that demonstrate an attenuation caused by the resonator and the Bragg scattering caused principally by the periodicity of the structure when used WFE method.

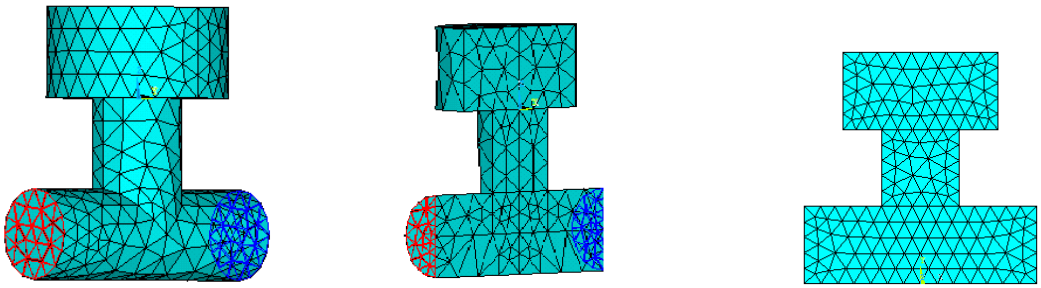

(a) (b) (c)

Figure 5. Model 2 mesh generated by ANSYS with geometry: (a) 3D; (b) F3D; (c) 2D.

Table 3. Number of nodes and elements in Model 2.

Geometry	Elements	Nodes
3D	3250	795
F3D	789	295
2D	319	195

Figure 6 shows the dispersion diagram of the Model 2. At low frequency band both methods (TMM and WFE) agrees, however as the frequency band increase TMM and WFE-2D present similar behavior with the dispersion curves close to each other. As expected WFE-3D and and F3D presents a good agreement for all frequency band, but are not close to TMM and WFE-2D. Two band gaps are identified, the first one can be identified as a locally resonant bandgap around f_{HR} = 273.14 Hz. The second one is a bandgap from the periodicity, which is located around the Bragg limit of f_{BL} = 572.1 Hz. It can be seen that both methods can identify the bandgap but presents differences in the bandgap position and width obtained with TMM & WFE-2D as compared to the WFE-3D & F3D, which are coincident. Now, as the cavity volume was reduced the third bandgap identified by TMM with Model 1 disappears. This result confirms the TMM limit, related to the plane wave hypothesis, since as the HR volume of cavity was reduced to the half it was enough for the result agrees with the others.

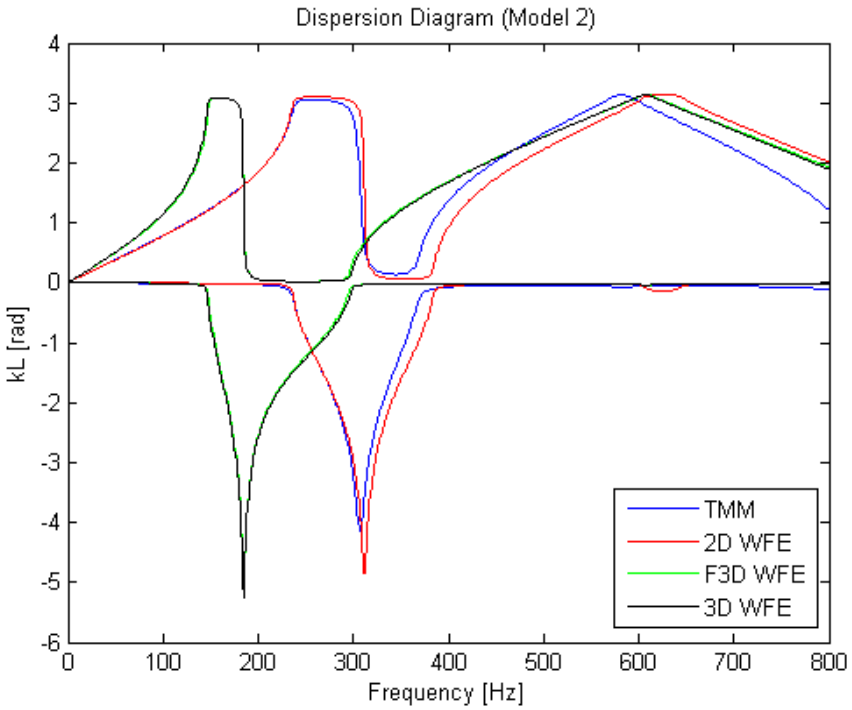

Figure 6. Dispersion diagram for Model 2 calculated by TMM and WFE with geometry: 2D, F3D and 3D.

For the next evaluation the Model 1 was modified to generate the Model 3. Model 3 consists of Model 1 with his cavity length increased by 25% (*lc* = 0.25 m). Table 4 shows the number of nodes and elements for Model 3 with geometry 3D, F3D and 2D. Figure 7 shows the Model 3 mesh generated by ANSYS with geometry 3D, F3D and 2D.

Table 4. Number of nodes and elements in Model 3.

Geometry	Nodes	Elements
3D	1162	5022
F3D	314	831
2D	298	507

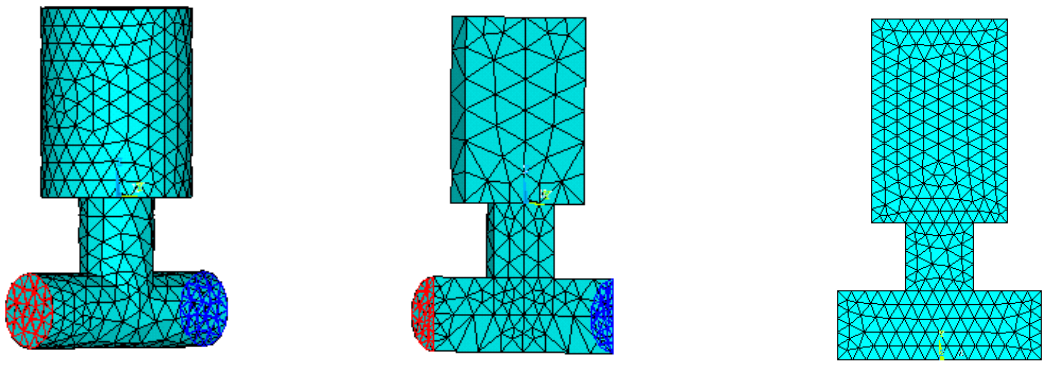

(a) (b) (c)

Figure 7. Model 3 mesh generated by ANSYS with geometry: (a) 3D; (b) F3D; (c) 2D.

Figure 8 shows the dispersion diagram of the Model 3. Figure 6 shows the dispersion diagram of the Model 2. Now at low frequency band results with TMM agree with WFE-2D, however as the frequency band increase they diverge. As expected WFE-3D and F3D presents a good agreement for all frequency bands, but are not close to TMM and WFE-2D.

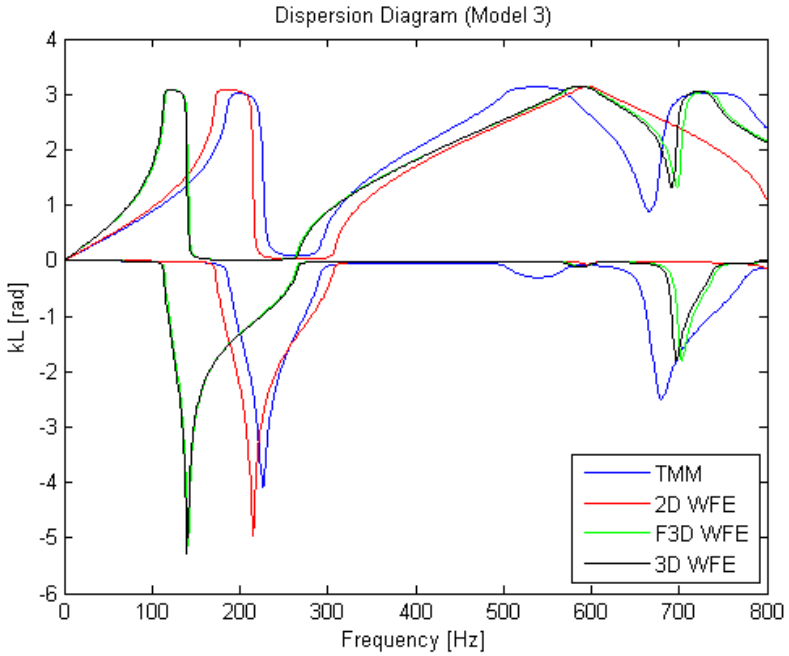

Figure 8. Dispersion diagram for Model 3 calculated by TMM and WFE with geometry: 2D, F3D and 3D.

Two band gaps are identified, the first one can be identified as a locally resonant bandgap around f_{HR} = 172.75 Hz. The second one is the same as before since the periodicity was not

changed (f_{BL} = 572.1 Hz). Similar to the results with Model 1 and 2 both methods can identify the bandgap, but presents differences in the bandgap position and width obtained with TMM & WFE-2D as compared to the WFE-3D & F3D, which are coincident. Now, as the cavity volume was enlarged the third false bandgap is identified by TMM, WFE-3D and F3D, but was not with WFE-2D. This result confirms the plane wave limit, since as the HR volume of cavity was enlarged TMM and WFE-3D models fail and only WFE-2D was unaffected.

5 CONCLUSION

The methodology used in this work to determine attenuation in ducts with a Helmholtz resonator can be used to optimize acoustic devices geometry to improve noise control. Two-dimensional and three-dimensional FE modeling of duct-HR system using acoustic mass and stiffness matrices extracted from a commercial software (ANSYS) were performed and processed using Matlab® to calculate dispersion diagrams of a periodic system with WFE method efficiently and precisely as compared with transfer matrix method (TMM).

The results for 03 duct-HR models varying the volume of the HR were evaluated related to its ability to identify the bandgaps position and width in frequency domain was evaluated. The results show that both methods TMM and WFE with different geometries (2D, 3D and F3D) are able to identify bandgaps generated by periodicity (Bragg effect) and locally resonators. Must be noticed that due the plane wave hypothesis assumed in all acoustic formulations evaluated, as the frequency band increase the dispersion diagram results can present false bandgaps.

Acknowledgements

The authors are partially supported by the Brazilian agencies CAPES, CNPq and FAPESP.

REFERENCES

ANSYS, 2013. *ANSYS Mechanical APDL Theory Reference Release 15.0*. Documentation for ANSYS. United States of America.

Beranek L. L., Vér I. L., 1992. *Noise and vibration control engineering: principles and applications*. John Wiley and Sons.

Cook, R.D., Malkus D.S., Plesha, M.E., & Witt, R.J., 2002. *Concepts and Applications of Finite Element Analysis*. John Wiley and Sons.

Dias, V. L., Dos Santos, J. M. C., & Arruda J. R. F., 2017. Passive control of noise propagation in tube systems using Bragg scattering. *XVII International Symposium on Dynamic Problems of Mechanics – DINAME*.

Duhamel, D., Mace, B.R., & Brennan, M.J., 2006 Finite element analysis of the vibrations of waveguides and periodic structures. *Journal of Sound and Vibration*, pp. 205–220.

Ichchou, M.N., Mencik, J.M., 2005. Multi-mode propagation and diffusion in structures through finite elements. *European Journal of Mechanics of Solids*, 24, pp. 877–898.

Kinsler, L.E., Frey, A.R., Coppens, A.B. & Sanders, J.V. 1982. *Fundamentals of Acoustics*. John Wiley and Sons.

Mace, B., Maconi, E., 2008. Modelling wave propagation in two-dimensional structures using finite element analysis. *Journal of Sound and Vibration*, 318, pp. 884–902.

Munjal, M.L. 1987. *Acoustics of Ducts and Mufflers*. John Wiley and Sons.

Singh S., Hansen C. H., & Howard C. Q., 2008. A detailed tutorial for evaluating in-duct net acoustic power transmission in a circular duct with an attached cylindrical Helmholtz resonator using transfer matrix method. *Congress of Acoustics and Sustainability – AAS* .